Published in final edited form as:
Radiother Oncol. 2012 June ; 103(3): 380–387. doi:10.1016/j.radonc.2012.03.014.

Kinomic profiling approach identifies Trk as a novel radiation modulator

John S. Jarboe[1,2,*], **Jerry J. Jaboin**[3,*], **Joshua C. Anderson**[2], **Somaira Nowsheen**[2], **Jennifer A. Stanley**[2], **Faris Naji**[4], **Rob Ruijtenbeek**[4], **Tianxiang Tu**[5], **Dennis E. Hallahan**[3], **Eddy S. Yang**[2], **James A. Bonner**[2], and **Christopher D. Willey**[†,1,2,6]

[1]Department of Biochemistry and Molecular Genetics, The University of Alabama at Birmingham [2]Department of Radiation Oncology, The University of Alabama at Birmingham [3]Department of Radiation Oncology, Washington University School of Medicine, St. Louis, MO [4]PamGene International B.V., Hertogenbosch, The Netherlands [5]Vanderbilt-Ingram Cancer Center, Vanderbilt University School of Medicine, Nashville, TN [6]Department of Cell Biology, The University of Alabama at Birmingham

Abstract

Background—Ionizing radiation treatment is used in over half of all cancer patients, thus determining the mechanisms of response or resistance is critical for the development of novel treatment approaches.

Materials and methods—In this report, we utilize a high-content peptide array platform that performs multiplex kinase assays with real-time kinetic readout to investigate the mechanism of radiation response in vascular endothelial cells. We applied this technology to irradiated human umbilical vein endothelial cells (HUVEC).

Results—We identified 49 specific tyrosine phosphopeptides that were differentially affected by irradiation over a time course of one hour. In one example, the Tropomyosin receptor kinase (Trk) family members, TrkA and TrkB, showed transient activation between 2–15 minutes following irradiation. When we targeted TrkA and TrkB using small molecule inhibitors, HUVEC were protected from radiation damage. Conversely, stimulation of TrkA using gambogic amide promoted radiation enhancement.

Conclusions—Thus, we show that our approach not only can identify rapid changes in kinase activity but also identify novel targets such as TrkA. TrkA inhibition resulted in radioprotection that correlated with enhanced repair of radiation-induced damage while TrkA stimulation by gambogic amide produced radiation sensitization.

[†]Correspondence to: Christopher D. Willey, MD, PhD, Department of Radiation Oncology, Department of Cell Biology, Department of Biochemistry and Molecular Genetics, The University of Alabama at Birmingham, HSROC 2232C, 619 19th St S, Birmingham, AL 35249-6832, cwilley@uab.edu, Telephone: 205-934-5670, Fax: 205-975-0784.
[*]indicates equal contribution as co-first authors

Presented at the 11th International Wolfsberg Meeting, 2009

CONFLICT OF INTEREST STATEMENT

Rob Ruijtenbeek is vice president of research at PamGene International and Faris Naji is also employed by PamGene International. The remaining authors have declared that no conflicts of interests exist.

Keywords

kinomics; Trk; DNA repair; radiation; tumor microvasculature

Introduction

The vasculature is crucial for tumor development, progression, and metastatic potential. The emergence of effective cancer therapeutics that function as anti-angiogenic agents [14] (such as bevacizumab and sunitinib) is a testament to the importance of the vasculature for the tumor microenvironment. Interestingly, the use of many of these anti-angiogenic agents has shown significant promise when combined with ionizing radiation [14]. Since radiation is used as cancer treatment for at least half of all cancer patients, combined modality therapy using anti-angiogenic agents with radiation can potentially impact a large population. Originally, it was thought that anti-vascular treatments would negatively impact radiation treatment since traditional radiobiology has shown that hypoxia causes radiation resistance [10]. However, work by Rakesh Jain [12] and others [23] have shown that anti-vascular treatment may improve blood flow within tumors by normalizing ineffective vascular dynamics which then allows chemotherapeutics to better permeate a tumor as well as improving oxygenation for radiation sensitization. However, vascular destruction (vasculitic therapy) should improve tumor control by simply eliminating the nutrients necessary for tumor preservation. Therefore, there are multiple potential therapeutic benefits that can be achieved with vascular targeting.

In terms of inherent radiosensitivity, the vascular endothelium is rather resistant to the effects of typical clinical doses of radiation, on the order of 2–3 Gy per fraction. Vascular destruction from radiation alone requires much higher doses of radiation. The prime example is stereotactic radiosurgery which can be used to treat arteriovenous malformations, primary and metastatic tumors. Single doses exceeding 15 Gy are given which results in ablation and necrosis of both tumor and blood vessels. The vastly different response to radiation based on dose suggests that differences exist in biological mechanisms such that the lower dose radiation (2–3 Gy) produces a survival pathway while the higher doses either overwhelm or do not stimulate the survival mechanism. Therefore, several groups [6,8,16,23] including ours have investigated the signaling pathways within the vascular endothelium to try to determine which ones are mediating radiation sensitivity.

Since many anti-angiogenic agents target tyrosine kinases, we wanted to examine the global tyrosine kinase activation profile induced by radiation treatment in vascular endothelium in search of potential new targets for modulating treatment response. Attempts at indirect kinomic assessment such as with reverse-phase protein microarrays have shown that basal phosphorylation levels of certain proteins in tumors have the potential for predicting treatment response for some molecularly targeted agents, and that compensatory signaling occurs in response to therapy [4]. We hypothesized that tyrosine kinase activation would also change in response to ionizing radiation. Although this is not a new concept, the detection of dynamically regulated proteins, such as kinases, has been challenging.

Many high-throughput technologies have been developed to make global biological assessments in hopes of identifying new hypotheses and targets for drug development. RNA interference (RNAi), genomics, and proteomics-based methods have shown promise in these types of studies. However, genomics and proteomics assays are limited in their ability to analyze kinase pathways, likely due to the fact that kinases are predominantly regulated by post-translational modification. Although RNAi methods may determine the consequence of loss of a kinase protein, small molecule inhibitors to kinases do not typically lead to “loss”

of the protein but actually inhibit their enzymatic activity. Therefore, “kinomic” analysis of biological systems provides a more direct measure of kinase pathways by determining changes in kinase activity (as phosphorylation events). The determination of protein phosphorylation status in response to treatment is a challenge due to the transient nature and complex milieu within the treated cells. To date, we are restricted in the number of phosphorylation events that can be studied at one time. Mass spectrometry has been used to examine post-translational modification for several years. However, detecting phosphorylation has been difficult due to the negative charge on the phosphate. This negative charge interferes with the detection of ionic species in this modality. Nevertheless, phosphoproteomic approaches have been developed such as immobilized metal affinity chromatography (IMAC) or immunoprecipitation with phosphotyrosine antibodies to select phosphorylated peptides that can then be identified by reverse-phased liquid chromatography-tandem mass spectrometry (LC-MS/MS) [2,20]. Certainly, progress has been made in identifying phosphorylated peptides in complex samples. However, this approach is expensive, time consuming, and statistically challenging. So, despite new algorithms and approaches for large-scale identification of phosphorylation sites, mass spectrometry is still limited in its throughput, particularly when serial measurements over time are required, as in treatment response studies for cancer therapeutics. As an alternative, we utilized a platform that measures phosphorylation events within a whole cell lysate kinase assay. This was achieved using a three-dimensional peptide chip microarray which overcomes some of the challenges that face mass spectrometry approaches.

Materials and methods

Reagents

HUVEC were purchased from Clonetics (San Diego, CA) and were limited to passages 3–6 for experimentation. HUVEC were grown in EBM-2 medium with supplementation using EBM-2 singlequots (Cambrex). Cells were incubated at 37°C in a 5% CO_2 incubator. Tropomyosin receptor kinase A (TrkA) inhibitor and K252a Trk family inhibitor were purchased from Calbiochem and Tocris, respectively. Gambogic amide was purchased from Biomol (Enzo Life Sciences Inc., Ann Arbor, MI).

HUVEC treatment and lysate preparation

HUVEC (passage 4) were grown in 12 × 10 cm tissue culture plates up to 80–90% confluence. The cells were serum starved using MCDB-131 supplemented with L-Glutamine and 0.2% BSA for 6 hours. The cells were then treated with either sham or 3 Gy irradiation (At a dose rate of 1.897 Gy/min) using a MARK IV ^{137}Cs irradiator (JL Shepard and Assoc) and then were incubated for 0, 2, 5, 15, 30, or 60 minutes at 37 °C and 5% CO_2. After the appropriate incubation time, the dishes were placed on ice and the medium was aspirated. The cells were washed twice with 4 ml ice cold 1xPBS. M-Per lysis buffer (Thermo Scientific) containing protease and phosphatase inhibitor cocktails (Sigma) was then added to each dish (150μl per 10cm dish) and incubated for 30 minutes on ice. The lysates were collected and vortexed for 20 sec followed by centrifugation at 10,000g for 30 min at 4 °C using an F2402 rotor. The supernatants were transferred to eppendorf tubes and immediately flash frozen in liquid nitrogen. Concentrations for each sample were determined using the BCA method (Thermo Scientific). This experiment was repeated 10 days later using a separate pool of HUVEC (“biological replicate”).

PamStation Kinomic Analysis

Kinomic profiling of HUVEC lysates prepared as described above was performed using a PamStation®96 microarray (PamGene International) with PTK PamChip® containing 144 consensus phospho-peptide sequences/well representing the tyrosine kinome. Each well of

the PamChips® were first blocked in 2% Bovine Serum Albumin (BSA). Following protein concentration determination (by BCA assay), 2–5 μg of protein were loaded per well of the PamChip® along with standard kinase buffer (PamGene), 400 μM ATP, and FITC-labeled anti-phospho-tyrosine antibodies (PamGene). Each biological replicate lysate was run in quadruplicate ("technical replicates"). The assay mix, containing the active kinases in the sample lysates, was pumped through the PamChip® wells allowing it to interact with the specific peptides that are immobilized in the chip. The degree of phosphorylation was measured in real time via the kinetic image capture program, Evolve (PamGene), that captured FITC labeled anti-phosphotyrosine antibody binding to each phosphorylated peptide substrate every 6 seconds for the length of the program (60 minutes). Following 60 min incubation, the signal intensities for each peptide were analyzed using BioNavigator Software (PamGene) as described below.

Kinomic Statistical Analysis

Cross-Gene error model takes variability data from a high-throughput system and estimates measurement precision. GeneSpring v. 7.3.1 software by Agilent Technologies was used to perform this analysis based on the sample replicate method for cross-gene error calculations which assumes that variability between "biological" replicates is similar for all phosphopeptides with similar measurement levels. K-means clustering of gene list 'Crossgene error model list' was based on the following interpretation(s): experiment 1 irradiated, Default Interpretation [mode 'Log of ratio', weight 1.0]. The parameters used: Number of clusters=4, Number of iterations=100, similarity metric of Pearson Correlation was performed and the data converged after 5 iterations.

Immunoprecipitation

HUVEC were serum starved in 0.2% serum for 5 hours prior to irradiation with 0 or 3 Gy. Lysates were immediately prepared in M-Per with protease and phosphatase inhibitors as above. 500 μg of total protein were combined with 40 μl of ProteinG/plus A agarose beads and were rotated at 4°C for 2.5 h. Ten μl of anti-TrK (Pan) polyclonal antibody (Cell Signaling Technology) was added and then rotated overnight at 4°C. Following cold lysis buffer washes (n=3), 4X SDS sample buffer was added and then boiled for 10 min. This was then run on SDS-PAGE with anti-PY20HRP immunoblotting according as described before [24].

Clonogenic survival assays

Clonogenic (colony formation) assays were performed as previously described [3] with minor modifications. HUVEC grown to 80% confluency were trypsinized and serially diluted to defined concentrations and plated in triplicate. The following day, cells were treated with either DMSO control, 5–50 nM TrkA inhibitor, 100 nM K252a, or 25 nM gambogic amide 1h prior to receiving 0–8 Gy. Cells were then incubated for 2 h and then medium was changed to regular growth medium. Ten to fourteen days later, cells were fixed with 70% ethanol and stained with 1% methylene blue. Colonies were counted and a surviving fraction (S.F.) was calculated by using the equation (number of colonies formed/number of cells plated)/(number of colonies for sham irradiated group/number of cells plated). The results were then plotted as mean and standard error of the mean in a semi-logarithmic format using Microsoft Excel software.

Immunofluorescence

HUVEC cells were cultured and seeded on sterile cover slips, exposed to DMSO control, 50 nM TrkA inhibitor, or 100 nM K252A inhibitor for 1hr, and subsequently treated with mock or 6 Gy using a 320 kV X-ray irradiator (Kimtron Inc., Woodbury, CT). Cells were then

incubated for 2hrs prior to changing the medium to regular growth medium. Immunohistochemistry was performed as previously described [18]. Briefly, cells were rinsed in phosphate buffered saline (PBS) and incubated for 5 minutes at 4°C in ice-cold cytoskeleton buffer (10mM Hepes/KOH, pH 7.4, 300mM sucrose, 100mM NaCl, 3mM $MgCl_2$) supplemented with 1mM PMSF, 0.5mM sodium vanadate and proteasome inhibitor (Sigma, 1:100 dilution) followed by fixation in 70% ethanol for 15 minutes. The cells were blocked and incubated with primary antibodies [1:500 dilution, Rad 51 (H-92), Santa Cruz Biotechnology, catalog # sc-8349, DNA PKcs phospho T2609, Genetex, catalog # GTX-24194, or phospho H2AX Ser139, Millipore, catalog # MI-07-164]. The secondary antibody was anti-rabbit Alexa Fluor 594–conjugated or anti-mouse Alexa Fluor 488-conjugated antibody (1:2000 dilution; Invitrogen). DAPI (Invitrogen, catalog # D21490) was used for nuclear staining. The cover slips were subsequently mounted onto slides with mounting media (Aqua poly mount, Polysciences, Inc. catalog # 18606) and analyzed via fluorescence microscopy (Carl Zeiss, Thornwood, NY). Positive and negative controls were included on all experiments. A total of 500 cells were assessed. For foci quantification, cells with greater than 10 foci were counted as positive according to the standard binning procedure [18,27,28]. Average foci per cell was also calculated for each condition.

Cell Cycle Analysis

HUVEC (2×10^5) were plated in 6-well dishes and allowed to adhere overnight. The following day they were treated with 50 nM of TrkA inhibitor, 100 nM of K252a or DMSO control for one hour. The cells were then irradiated with 6 Gy and the media was replaced two hours post-irradiation. The cells were harvested by trypsinization at the indicated time points, the trypsin was neutralized with media and the cells were collected by centrifugation at 1000 rpm for 10 minutes. The cells were re-suspended in 1 ml of cold PBS and were then fixed with the addition of 4 ml of −20°C ethanol at 4°C overnight. The next day, the cells were again collected by centrifugation and the fixative was aspirated. The cells were then re-suspended in 300 μl PBS + 1 μl RNAse (25 mg/ml) and incubated at 37°C for 30 minutes. 30 μl propidium iodide (in PBS 100 μg/ml final concentration) was added to each sample. Flow cytometry was performed at the UAB Flow Cytometry Center for Aids Research (CFAR) Core. These were performed in triplicate.

Results

The microarray system described here utilizes an aluminum oxide porous material that contains long branched interconnected capillaries, providing tremendous surface area for substrate immobilization on the order of 500 fold the capacity of two-dimensional arrays. The PTK PamChip® (PamGene International) array was generated using phosphorylatable tyrosine-containing peptide sequences representing phosphosites of the tyrosine kinome. Each phosphosite peptide contains 13 residues (each with phosphorylatable tyrosines) derived from consensus sequences with an additional two N-terminal residues that are linked to the microarray material (See Supplemental table 1). By passing whole cell or tissue lysates prepared in kinase buffer (containing ATP) over the microarray material, a kinase reaction will take place within the peptide-laden metal oxide pores. Using a fluorescently labeled anti-phosphotyrosine antibody (PY20), CCD camera imaging can detect and quantify differential phosphorylation intensity during the course of the kinase assay (Fig. 1). The PTK PamChip® contains 144 phosphorylatable peptide substrates that survey the entire tyrosine kinome. Therefore, this platform provides the opportunity to evaluate numerous conditions simultaneously in a high-throughput format.

We selected the primary culture cell line, human umbilical vein endothelial cells (HUVEC), a well studied model of vasculature, to test the hypothesis that kinomic profiling could elucidate mechanisms of sensitivity/resistance to radiation treatment. In order to perform the

kinomic analysis, optimization for cell type and conditions was required. We first optimized protein loading by performing kinomic profiling of untreated HUVEC using both 2 μg and 5 μg total protein per well (Supplemental Fig. 1). Based on those studies, we selected 3 μg as the optimal protein amount for loading/well. We next optimized blocking conditions with 0, 0.2 and 2% blocking solution. In this case, 0.2% bovine serum albumin was selected. Once optimal conditions were determined, a radiation time course experiment was performed.

Due to the inherent variability of cell based experimental models, particularly in primary culture cells such as HUVEC which are derived from a pool of donors, a thorough replication approach was pursued. We treated HUVEC (Passage 4) with either sham or 3 Gy irradiation and then prepared whole cell lysates 0, 2, 5, 15, 30, or 60 minutes post-irradiation (Fig. 2A). These samples were considered the first “biological” replicate. Ten days later, we repeated the exact same procedure using a separate HUVEC source to obtain the second biological replicate. These biological replicates were then analyzed using the PamStation® 96 (PamGene International). Pre-fabricated PTK PamChips® with 144 spots in each well containing consensus phosphopeptide sequences/per well were analyzed following flow-through incubation of cell lysates prepared from the HUVEC biological replicates loaded in quadruplicate (Four “technical” replicates) (Fig. 2B). Fluorescent-labeled anti-phosphotyrosine antibodies (PY20-FITC) were incubated at 37°C with these lysates in the presence of 400 μM ATP and kinase buffer with CCD imaging every 6 seconds for 60 minutes. Kinetic curves were generated but only end-level values (Fig. 2C) were used for statistical analysis. As such, 13,842 end-level data points were analyzed using a tandem system of BioNavigator (PamGene International) and GeneSpring (Agilent) software modules. A cross gene error model identified 49 phosphopeptides that passed initial screening (See Supplemental Fig. 3). Normalization was then performed by averaging the signal for the 4 technical replicates and taking the ratio [mean peptide signals irradiated group]/[median control at same time point]. K-means clustering was then performed which identified four distinct sets of peptides. This is shown graphically (Fig. 3A and Supplemental Fig. 2) in which each blue line represents a distinct phosphopeptide with vertical lines delineating the time course. Normalized intensity for each phosphopeptide is shown on a logarithmic scale for each biological replicate experiment. As can be seen, the sham irradiation groups (GY0-1 and GY0-2) show only minimal changes in normalized intensity. In contrast, several phosphopeptides in the irradiated group (GY3-1 and GY3-2) show significant changes, some over an order of magnitude. Peptide set 2 (Fig. 3A and Supplemental Fig. 2B) had robust and rapid phosphorylation events which were very consistent between the two biological replicate experiments. Technical variability was quite small as the coefficient of variation was below 20% in a very high percentage of the samples that implies very good reproducibility (Data not shown). This is also apparent in the error bars shown for NTRK1_Y496 (Figure 3B). As such, we focused our validation experiments on this group of 10 genes (See Supplemental Fig. 3, Peptide Set 2). Of this group, two phosphopeptides were of the same family and corresponded to the autophosphorylation sequences of the nerve growth factor receptors, TrkA (NTRK1) and TrkB (NTRK2). We confirmed this by subjecting HUVEC to sham (0 Gy) or 3 Gy irradiation followed by immunoprecipitation of Trk using a pan-Trk antibody. These lysates were then run on SDS-PAGE and analyzed for phosphorylation using anti-PY20HRP immunoblot. As shown in Fig. 3B, Trk phosphorylation is induced by 3 Gy irradiation.

Trk, the Tropomyosin receptor kinase, is a high-affinity receptor tyrosine kinase for neurotrophins (NT) of the nerve growth factor family ($Kd=10^{-11}M$ for NGF). Trk receptors are known proto-oncogenes that play key roles in differentiation and apoptosis during neural development. Molecular roles for this family are found in cancers of the central nervous system, papillary thyroid, colon cancer and acute myelogenous leukemia. Although Trk receptors have been detected in HUVEC [5], little is known about their function. When

TrkA specific inhibitor (TrkA inhibitor) or pan-Trk inhibitor (K252a) was used to pretreat HUVEC prior to irradiation with 0, 3, 5, or 8 Gy in clonogenic assays, these inhibitors produced radiation protection at nanomolar ranges (TrkA Inhibitor, p=0.0024; K252a, p=0.0355 at 5 Gy) (Fig. 3C).

Because as little as one unrepaired DNA double strand break (DSB) is lethal to a cell, we next hypothesized that enhanced DNA repair may play a role in Trk inhibitor-induced radioprotection. Thus, we analyzed DNA damage and repair kinetics in these cells. γ-H2AX foci levels, indicative of DNA DSBs, were measured following treatment with the Trk inhibitors. As shown in Fig. 4A and Supplemental Figure 4, Trk inhibition with either TrkA inhibitor or K252a prior to irradiation produced a statistically significant ($p<0.0001$) reduction in γ-H2AX foci formation, particularly at 30 minutes, and 1 hour post-radiation. Of note, we could detect reduced γH2AX foci as late as 6 hours post irradiation for the TrkA inhibitor treated cells ($p<0.01$). By 24 hours, foci formation returned to basal levels. Having demonstrated a faster reduction in γH2AX foci, which supports an effect of the inhibitors on DNA repair, we examined the impact of Trk inhibition on the two major DNA repair pathways, homologous recombination (HR) and non-homologous end joining (NHEJ). Fig. 4B shows HR repair via quantitation of Rad51 foci, a well-established marker for HR-mediated repair, following treatment with Trk inhibition and radiation. Although there was a slight reduction in Rad51 foci formation following treatment with the inhibitors, it was not significantly different overall (p=0.7498). However, we did identify a statistically significant increase in phospho-DNA PK foci levels ($p<0.0001$) indicative of proficient NHEJ-mediated repair. Maximal induction in phospho-DNA Pk was observed immediately as well as 30 minutes following radiation in both TrkA inhibitor treated ($p<0.05$ and <0.01, respectively) and K252a treated ($p<0.001$ and <0.0001, respectively) cells (Fig. 4C). This correlates well with the decrease in γ-H2AX foci formation observed at the early time points. These results suggest that in irradiated vascular endothelial cells, radioprotection from Trk inhibition may be due to enhanced NHEJ-mediated repair.

Based on the above results, we hypothesized that stimulation of the Trk receptors would sensitize HUVEC to radiation. As such, we performed additional clonogenic assays following stimulation of TrkA with gambogic amide, a known potent and specific agonist for TrkA [13]. Pretreatment of HUVEC with 25 nM gambogic amide promoted radiation enhancement (p=0.006 at 2 Gy) (Fig. 5).

Discussion

NTs, including nerve growth factor (NGF), brain-derived neurotrophic factor (BDNF), and NT-3, -4/5, and -6 are critical to the development of the human nervous system. Moreover, NTs are important for survival and maintenance of neurons [25]. NT receptors include both the low-affinity p75NTR as well as the high-affinity Trk family of receptors, which include TrkA, B, and C. NGF preferentially binds to TrkA, BDNF and NT-4/5 bind TrkB, and NT-3 interacts with TrkC [17]. Following NT binding, Trks homodimerize and autophosphorylate specific tyrosine residues for receptor kinase activation as well as for creating docking sites for protein-protein interaction [7]. Downstream signals from Trks are known to influence PI3 Kinase, Akt, PKC, Ras, and Erk. As such, Trk signaling can affect apoptosis, growth and differentiation pathways which are critical targets for cancer therapeutics. Our work presented here has identified transient radiation-induced Trk activation, and that Trk inhibition promotes radioprotection while TrkA stimulation enhances radiation-induced death in vascular endothelial cells.

Much of what is known about Trk comes from studies of neuroblastoma and medulloblastoma, where Trk expression levels are prognostic (Reviewed in [21]). In normal

neurons, all three Trks are expressed and low levels are detectable in astrocytes. However, data surrounding Trk in glioma are controversial. Trks have been detected in astrocytic gliomas but not oligodendrogliomas [26] with higher levels of TrkA and B expression in lower grade lesions, suggesting that these Trks may be involved in tumorigenesis. While one group that identified TrkA in the glioblastoma cell lines, U251, U87, and U373, found that the Trk inhibitor, K252a, can inhibit NGF-stimulated proliferation [22], others have shown that overexpression of TrkA in U251MG cell lines can elicit differentiation and growth inhibition [15]. As such, the role(s) of Trk in glioma remains unclear.

More recently, investigations into the importance of Trk in non-CNS tissues have developed. Interestingly, Trk signaling has been implicated in Wilms Tumor, multiple myeloma, thyroid, lung, pancreas and prostate cancer [7,17]. Moreover, evidence suggests that TrkB can promote neoangiogenesis [7] while NGF stimulation of TrkA promotes angiogenesis *in vivo* [5]. Taken together, Trk appears to be an important player in tumor development as well as response to therapy. Because we saw similar results with both the TrkA specific inhibitor and the pan-Trk inhibitor K252a, we suspect that TrkA may be the key family member in terms of radiation response. Our findings are particularly striking considering that Trk inhibitors, such as K252a, tend to promote cell death [19] rather than promote a protective affect as we show here. However, it should be noted that the doses of K252a that have been used in such studies are 10-fold higher than the doses used in our work.

The direct evaluation of kinase activity described herein provides the proof of principle for using kinomic technology for time course and treatment response studies. Indeed, despite detecting only a transient Trk activation with irradiation, these studies demonstrate that Trk activity promotes radiation sensitization in vascular endothelial cells since Trk stimulation enhanced radiation effect while Trk inhibition radioprotected. As such, the Trk family may be a new class of molecular targets for modulating radiation effect in vasculature. The radioprotection that is promoted through TrkA inhibition and Trk family inhibition (K252a) appears to involve enhanced DNA DSB repair as we detected a faster rate of resolution of γH2AX foci in the irradiated samples. This enhanced repair utilizes the NHEJ pathway based on enhanced phospho-DNA-PKcs foci formation following radiation in the Trk inhibited cells. We were unable to detect significant differences in Rad-51 foci levels between control and treated cells suggesting that HR-mediated repair may not be essential in mediating this radioprotective response.

Although our studies were limited to radiation treatments, this kinomic profiling strategy can be applied to chemotherapeutics and molecularly targeted agents. Currently, prospective trials are investigating whether or not the genomic “signatures” of patient tumors can more accurately determine prognosis than standard clinicopathological features. Unfortunately, molecular biomarker utilization for predicting response to molecularly targeted agents has been fraught with problems. For example, EGFR expression levels have not correlated with EGFR kinase inhibition response consistently among disease sites [1,9], do not necessarily equate with activation [11], and identification of kinase mutations has further complicated studies for predicting response [1]. Thus, a kinase activity-based assessment provides a more rational approach to the study of kinase inhibitors. Indeed, by using a kinase assay, resistance from any source, be it overexpression, mutation, or other “short-circuits” should be detectable. This information could not only provide prognostic and predictive information but also generate hypotheses regarding pathways for treatment resistance. The specific findings of this report suggest that further work is warranted to determine whether the manipulation of TrkA expression may lead to new cancer therapeutic strategies.

Supplementary Material

Refer to Web version on PubMed Central for supplementary material.

Acknowledgments

We would like to especially thank Dirk Pijnenburg (PamGene International) for helping with the quality assurance of the PamStation data that were used for this manuscript.

Grant Support: PamGene International collaborative agreement, NIH/NCI, R01-CA1256757 (to D.E.H), R21-CA128456 (to D.E.H), R01-CA112385 (to D.E.H), 2R01-CA89674 (to D.E.H), P50-CA90949 (to D.E.H), University of Alabama Health Services Foundation General Endowment Fund Scholar Award (to C.D.W.). IMPACT Award from the Department of Radiation Oncology, University of Alabama-Birmingham Comprehensive Cancer Center, University of Alabama-Birmingham School of Medicine (to E.S.Y.)

References

1. Barton S, Starling N, Swanton C. Predictive molecular markers of response to epidermal growth factor receptor(EGFR) family-targeted therapies. Curr Cancer Drug Targets. 2010; 10:799–812. [PubMed: 20718710]
2. Beausoleil SA, Villen J, Gerber SA, Rush J, Gygi SP. A probability-based approach for high-throughput protein phosphorylation analysis and site localization. Nat Biotechnol. 2006; 24:1285–1292. [PubMed: 16964243]
3. Bonner JA, Trummell HQ, Willey CD, Plants BA, Raisch KP. Inhibition of STAT-3 results in radiosensitization of human squamous cell carcinoma. Radiother Oncol. 2009; 92:339–344. [PubMed: 19616333]
4. Boyd ZS, Wu QJ, O'Brien C, et al. Proteomic analysis of breast cancer molecular subtypes and biomarkers of response to targeted kinase inhibitors using reverse-phase protein microarrays. Mol Cancer Ther. 2008
5. Cantarella G, Lempereur L, Presta M, et al. Nerve growth factor-endothelial cell interaction leads to angiogenesis in vitro and in vivo. Faseb J. 2002; 16:1307–1309. [PubMed: 12154004]
6. Cuneo KC, Tu T, Geng L, Fu A, Hallahan DE, Willey CD. HIV protease inhibitors enhance the efficacy of irradiation. Cancer Res. 2007; 67:4886–4893. [PubMed: 17510418]
7. Desmet CJ, Peeper DS. The neurotrophic receptor TrkB: a drug target in anti-cancer therapy? Cell Mol Life Sci. 2006; 63:755–759. [PubMed: 16568244]
8. Fukumura D, Jain RK. Tumor microvasculature and microenvironment: targets for anti-angiogenesis and normalization. Microvasc Res. 2007; 74:72–84. [PubMed: 17560615]
9. Gurtner K, Deuse Y, Butof R, et al. Diverse effects of combined radiotherapy and EGFR inhibition with antibodies or TK inhibitors on local tumour control and correlation with EGFR gene expression. Radiother Oncol. 2011; 99:323–330. [PubMed: 21665304]
10. Hall, EJ.; Giaccia, AJ. Radiobiology for the radiologist. Philadelphia: Lippincott Williams & Wilkins; 2006.
11. Halle C, Lando M, Sundfor K, Kristensen GB, Holm R, Lyng H. Phosphorylation of EGFR measured with in situ proximity ligation assay: Relationship to EGFR protein level and gene dosage in cervical cancer. Radiother Oncol. 2011 Epub.
12. Jain RK. Normalization of tumor vasculature: an emerging concept in antiangiogenic therapy. Science. 2005; 307:58–62. [PubMed: 15637262]
13. Jang SW, Okada M, Sayeed I, et al. Gambogic amide, a selective agonist for TrkA receptor that possesses robust neurotrophic activity, prevents neuronal cell death. Proc Natl Acad Sci U S A. 2007; 104:16329–16334. [PubMed: 17911251]
14. Kim DW, Huamani J, Fu A, Hallahan DE. Molecular strategies targeting the host component of cancer to enhance tumor response to radiation therapy. Int J Radiat Oncol Biol Phys. 2006; 64:38–46. [PubMed: 16377414]
15. Kokunai T, Iguchi H, Tamaki N. Differentiation and growth inhibition of glioma cells induced by transfer of trk A proto-oncogene. J Neurooncol. 1999; 42:23–34. [PubMed: 10360476]

16. Manegold PC, Paringer C, Kulka U, et al. Antiangiogenic Therapy with Mammalian Target of Rapamycin Inhibitor RAD001 (Everolimus) Increases Radiosensitivity in Solid Cancer. Clin Cancer Res. 2008; 14:892–900. [PubMed: 18245553]

17. Nakagawara A. Trk receptor tyrosine kinases: a bridge between cancer and neural development. Cancer Lett. 2001; 169:107–114. [PubMed: 11431098]

18. Nowsheen S, Bonner JA, Yang ES. The poly(ADP-Ribose) polymerase inhibitor ABT-888 reduces radiation-induced nuclear EGFR and augments head and neck tumor response to radiotherapy. Radiother Oncol. 2011; 99:331–338. [PubMed: 21719137]

19. Perez-Pinera P, Hernandez T, Garcia-Suarez O, et al. The Trk tyrosine kinase inhibitor K252a regulates growth of lung adenocarcinomas. Mol Cell Biochem. 2007; 295:19–26. [PubMed: 16862449]

20. Rush J, Moritz A, Lee KA, et al. Immunoaffinity profiling of tyrosine phosphorylation in cancer cells. Nat Biotechnol. 2005; 23:94–101. [PubMed: 15592455]

21. Schramm A, Schulte JH, Astrahantseff K, et al. Biological effects of TrkA and TrkB receptor signaling in neuroblastoma. Cancer Lett. 2005; 228:143–153. [PubMed: 15921851]

22. Singer HS, Hansen B, Martinie D, Karp CL. Mitogenesis in glioblastoma multiforme cell lines: a role for NGF and its TrkA receptors. J Neurooncol. 1999; 45:1–8. [PubMed: 10728904]

23. Taguchi E, Nakamura K, Miura T, Shibuya M, Isoe T. Anti-tumor activity and tumor vessel normalization by the vascular endothelial growth factor receptor tyrosine kinase inhibitor KRN951 in a rat peritoneal disseminated tumor model. Cancer Sci. 2008

24. Tu T, Thotala D, Geng L, Hallahan DE, Willey CD. Bone marrow X kinase-mediated signal transduction in irradiated vascular endothelium. Cancer Res. 2008; 68:2861–2869. [PubMed: 18413754]

25. Wadhwa S, Nag TC, Jindal A, Kushwaha R, Mahapatra AK, Sarkar C. Expression of the neurotrophin receptors Trk A and Trk B in adult human astrocytoma and glioblastoma. J Biosci. 2003; 28:181–188. [PubMed: 12711810]

26. Wang Y, Hagel C, Hamel W, Muller S, Kluwe L, Westphal M. Trk A, B, and C are commonly expressed in human astrocytes and astrocytic gliomas but not by human oligodendrocytes and oligodendroglioma. Acta Neuropathol. 1998; 96:357–364. [PubMed: 9797000]

27. Yang ES, Nowsheen S, Wang T, Thotala DK, Xia F. Glycogen synthase kinase 3beta inhibition enhances repair of DNA double-strand breaks in irradiated hippocampal neurons. Neuro Oncol. 2011; 13:459–470. [PubMed: 21398658]

28. Yang ES, Wang H, Jiang G, et al. Lithium-mediated protection of hippocampal cells involves enhancement of DNA-PK-dependent repair in mice. J Clin Invest. 2009; 119:1124–1135. [PubMed: 19425167]

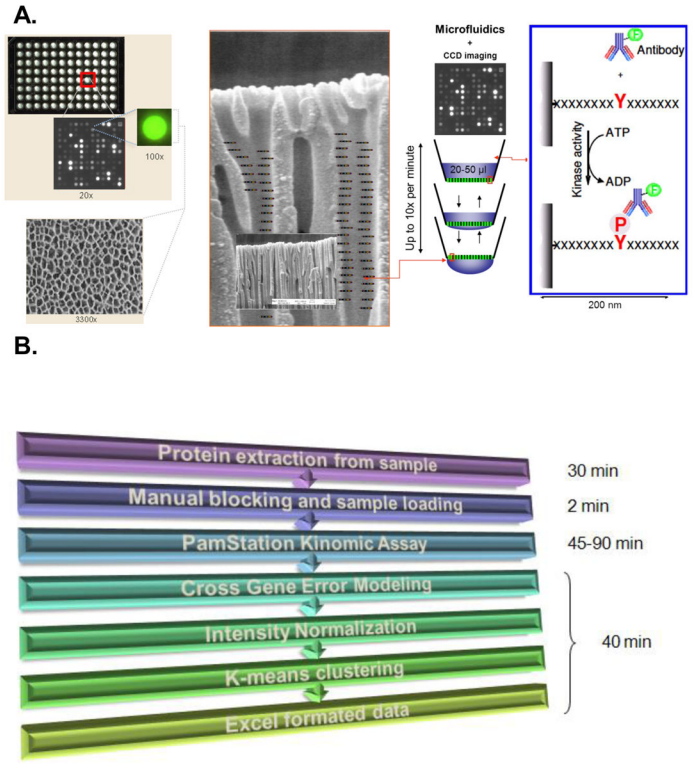

Figure 1. PamGene Array Technology

A) The PamChip®96 Array contains 96 spots/chip with each spot on the microarray containing up to 400 putative substrates allowing for multiplex analysis. The array is made of a porous aluminum oxide material 60 μm thick with interconnected capillaries having 500 X surface area of 2D arrays. This shows an enlarged schematic of the capillaries with peptide substrates indicated. In this example, the substrates are peptide sequences containing consensus tyrosine phosphorylation sites representing the tyrosine kinome. Lysates containing active kinases are pumped through the pores and phosphorylate specific peptides. The degree of phosphorylation is measured in real time by fluorescently labeled phospho-antibody binding detected by CCD cameras. See Materials and Methods for additional detail. **B)** *PamStation® flow chart with estimated time required:* Sample preparation requires only 30 minutes of time. The actual microarray analysis utilizes manual blocking of the chip and application of the sample (requiring about 2 minutes) followed by a fully automated analysis by the PamStation® (requiring 45–90 minutes). Lastly, data analysis is also automated such that annotated and quantified raw data, initial velocities and end levels, and coefficient of correlation for each readout can be obtained in exportable format (such as Excel) within 40 minutes.

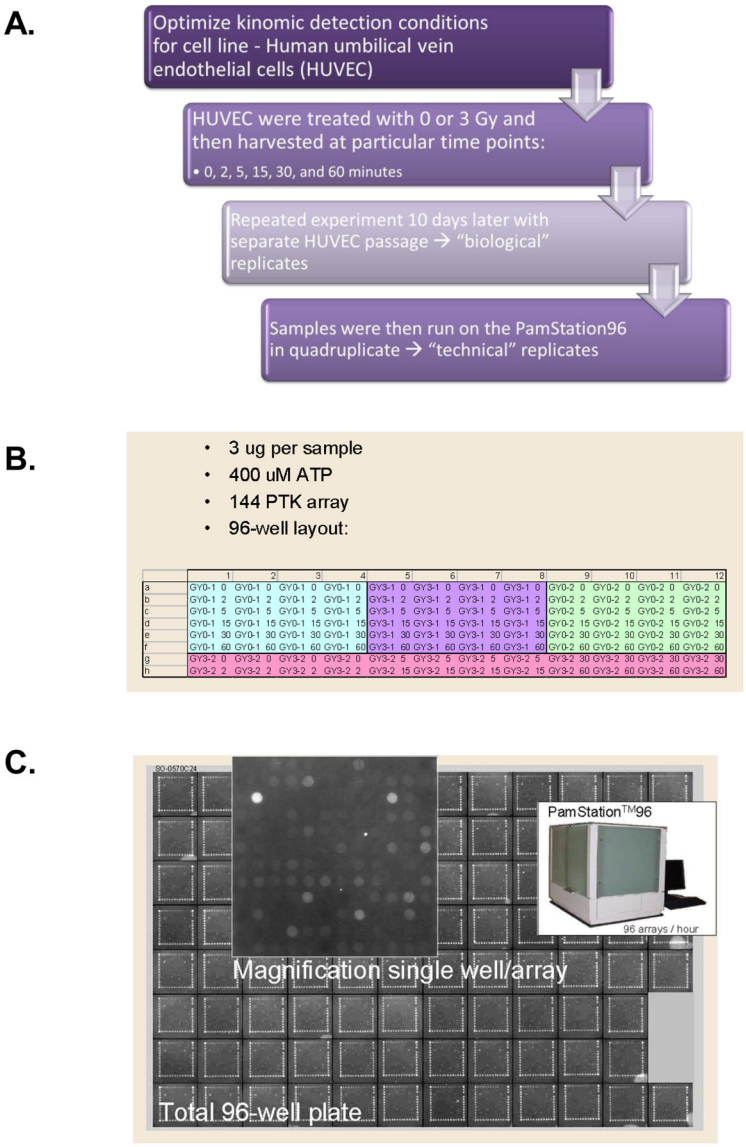

Figure 2. Kinomic evaluation of irradiated human umbilical vein endothelial cells

A) HUVEC were treated with 0 or 3 Gy irradiation and incubated for 0, 2, 5, 15, 30, or 60 min. Lysates were then prepared for PamStation® kinomic analysis of 144 specific tyrosine-containing peptides as described in Materials and methods. **B)** 96 well microtiter plate arrangement and kinase assay description. **C)** Last image of raw data captured on the PamStation®96.

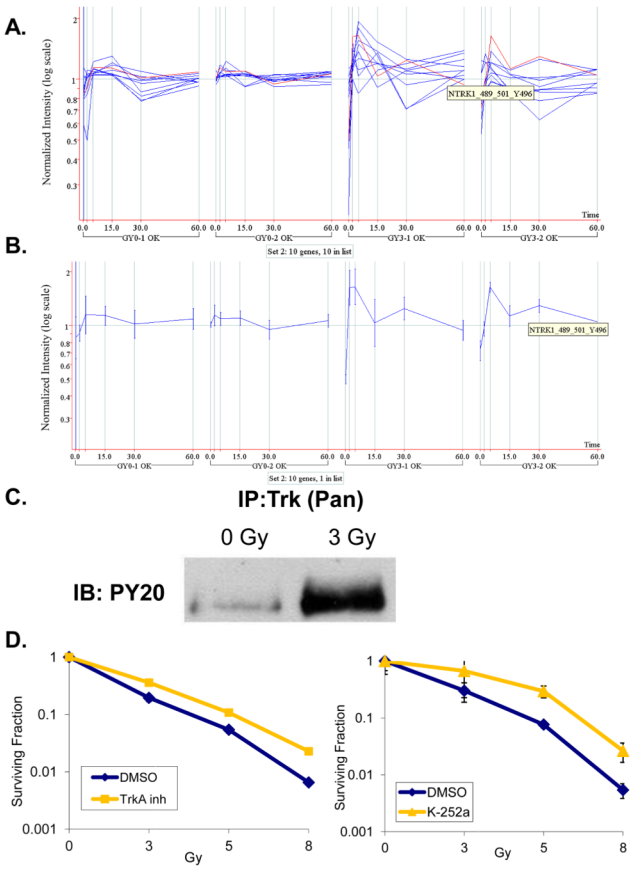

Figure 3. Radiation-induced Trk activation and impact of Trk inhibition on radiation response

A) Peptide set 2 is shown with normalized intensity (log scale) of phosphorylation of individual peptides after 0 (GY0-1 and -2) or 3 Gy (GY3-1 and -2) represented by a blue line at each time point (vertical lines). Highlighted in red is a single peptide of set 2 representing the phospho-site of NTRK1, also known as TrkA, which is shown separately in **B)** with standard error shown. **C)** A pan-Trk antibody was used to immunoprecipitate (IP) Trk in irradiated (3 Gy) and sham treated (0 Gy) HUVEC which were then subject to SDS-PAGE and immunoblotting (IB) for phosphotyrosine (PY20). **D)** The TrkA inhibitor from Calbiochem (Left Panel), or the pan-Trk inhibitor, K-252a, (Right Panel) was used to treat HUVEC 1 h prior to irradiation (0–8 Gy). Defined cell numbers were plated for each condition and incubated for 10 days. Surviving fraction of colonies formed were plotted (semi-log format) following normalization for plating efficiency (surviving fraction at 0 Gy). Standard error of the mean is indicated for each dose of irradiation.

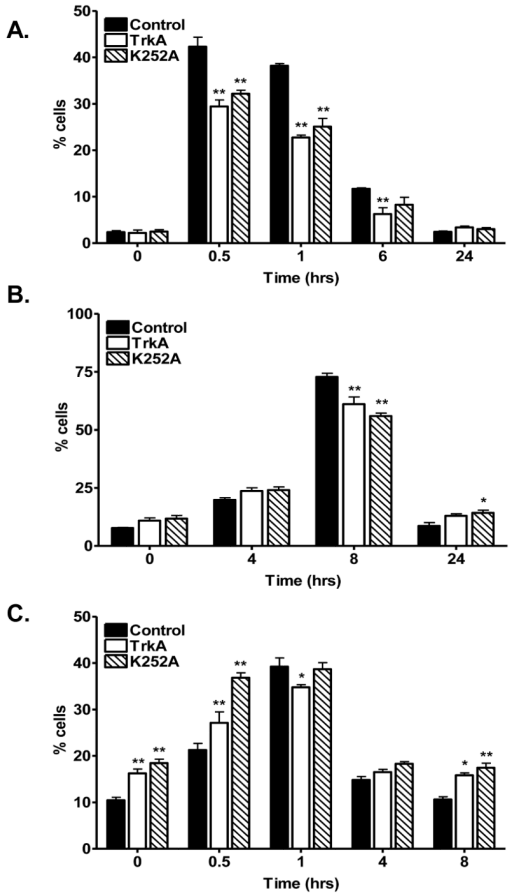

Figure 4. Trk inhibition promotes enhanced DNA repair following irradiation

HUVEC cells plated on sterile cover slips were treated with either vehicle control (DMSO) or TrkA inhibitor (TrkA, 50 nM) or pan-Trk inhibitor (K252a, 100 nM) for 1 hour followed by 6 Gy or mock irradiation. Cells were incubated for the indicated times prior to immunohistochemical staining for **A)** γ-H2AX foci, a commonly used marker for DSBs. **B)** Rad51 foci, marker for HR-mediated repair. **C)** phospho-DNA-PKcs foci, a marker for NHEJ-mediated DNA repair. Shown is the representative data of 3 independent experiments with the % of cells (mean +/− SEM) with > 10 foci (*, $p<0.05$, **, $p<0.01$).

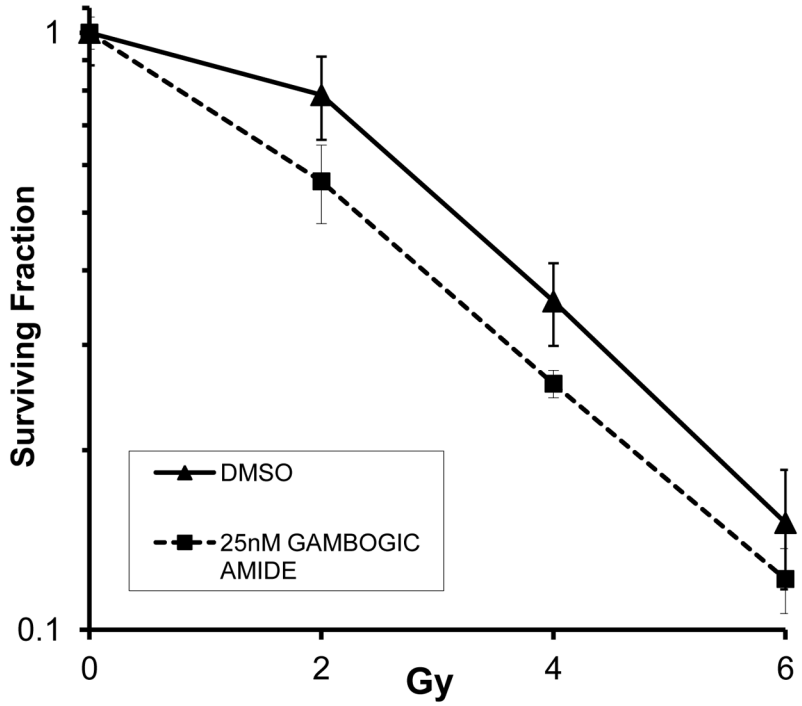

Figure 5. TrkA stimulation promotes radiosensitization

The TrkA agonist, gambogic amide (25 nM) was used to treat HUVEC 1 h prior to irradiation (0, 2, 4, or 6 Gy). Defined cell numbers were plated for each condition and incubated for 10 days. Surviving fraction of colonies formed were plotted (semi-log format) following normalization for plating efficiency (surviving fraction at 0 Gy). Standard error of the mean is indicated for each dose of irradiation.